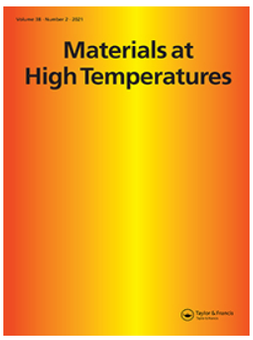

Materials at High Temperatures

ISSN: (Print) (Online) Journal homepage: https://www.tandfonline.com/loi/ymht20

Comparison of the corrosion performance of alloys HP40 and T22 exposed to molten salts at high temperature

Cecilia Cuevas Arteaga, Oscar Sotelo-Mazón, José Alfredo Rodríguez & Christian Marisol Clemente

To cite this article: Cecilia Cuevas Arteaga, Oscar Sotelo-Mazón, José Alfredo Rodríguez & Christian Marisol Clemente (2021) Comparison of the corrosion performance of alloys HP40 and T22 exposed to molten salts at high temperature, Materials at High Temperatures, 38:2, 123-138, DOI: 10.1080/09603409.2021.1893956

To link to this article: https://doi.org/10.1080/09603409.2021.1893956

Published online: 27 Feb 2021.

MATERIALS AT HIGH TEMPERATURES
2021, VOL. 38, NO. 2, 123–138
https://doi.org/10.1080/09603409.2021.1893956

Taylor & Francis
Taylor & Francis Group

RESEARCH ARTICLE

Comparison of the corrosion performance of alloys HP40 and T22 exposed to molten salts at high temperature

Cecilia Cuevas Arteaga[a], Oscar Sotelo-Mazón[b], José Alfredo Rodríguez[a] and Christian Marisol Clemente[c]

[a]Centro De Investigación En Ingeniería Y Ciencias Aplicadas; [b]Facultad De Ciencias Químicas E Ingeniería Universidad Autónoma Del Estado De Morelos Av. Universidad 1001, México; [c]Instituto De Ingeniería Y Tecnología, Universidad Autónoma De Ciudad Juárez, Cd. Juárez, Chih., México

ABSTRACT

The molten salt corrosion performance of SS-HP40 with high Cr content and carbon steel T22 with low Cr content were investigated. The corrosion behavior was obtained using three techniques: potentiodynamic polarisation curves (PC), electrochemical noise (EN) and the mass loss method (ML). XRD and SEM were utilized to characterize the oxide scales formed over the metallic surfaces. Alloys were exposed to 80% mol V_2O_5-20Na_2SO_4 mixture at 550°C and 650°C during 5 days. The corrosion rates of EN and ML agreed, showing to be thermally activated. SEM images showed that both materials suffered pitting corrosion in spite of HP40 has a great content of Cr. This result was due to high vanadium molten salt is very oxidant and acid, favoring a major dissolution of the Cr_2O_3 presents on HP40 and Fe_2O_3 formed on T22. Secondary corrosion products at low fusion points lead an increase in fluidity, which exacerbates the oxidation reactions.

ARTICLE HISTORY
Received 4 July 2019
Accepted 11 February 2021

KEYWORDS
Molten salt; high temperature; localised corrosion; electrochemical noise; mass loss method

INTRODUCTION

Due to the reduction of high-grade fuels but especially for economic reasons, residual fuel oil of low quality is greatly used in boilers of power generation plants [1,2], that is why fuel ash corrosion is well known as a form of attack caused by molten salts at high temperatures. Molten salts compounds melt between 500°C and 600°C and higher causing dissolution of the protective oxide scales of the metal alloys. This phenomenon can also be seen in gas turbines, aircraft and chemical process systems [1,3–5], which use residual fuel oils that during combustion produce compounds formed by sulphur, vanadium and sodium creating sulphate and vanadate salts [4–7], and other more complex mixtures coming from these primary species, which are extremely corrosive at temperatures in the range of 600°C–1050°C decreasing the lifetime of materials [8,9]. This type of corrosion is called high-temperature corrosion by molten salts or hot corrosion (HC) [3,4,10]. Boilers are essential elements of power generation plants, and HC occurs on the fireside of the heated surfaces of superheaters or reheaters, whose systems are primarily constructed of carbon steel materials of low chromium [1,11] and temperatures oscillate between 600°C and 650°C. This type of corrosion is also called vanadium attack, since there is evidence that vanadium contributes to the corrosion of metallic surfaces at high temperatures [12–14]. Since boiler systems are mainly made of carbon steel, corrosion is expected to be high, which can result in forced shutdowns [1]. Sulphur can diffuse through a porous oxide layer crossing a depleted metal surface, producing an internal degradation such as intergranular sulfidation, whereas the acidic oxide V_2O_5 can lead to fluxing mechanism of the metallic oxides formed over the surfaces [15]. Control of high-temperature molten salts corrosion by materials selection has been partially successful through the use of heat-resistant iron and nickel base alloys with high chromium content [16,17]. Cr has been the most used element in order to improve the corrosion properties of alloy, nevertheless, in some cases the cost of alloys with high content of good corrosion-resistant elements such as Cr, Al and/or Si is very high. Low alloy steels are commonly used in many industrial plants, therefore, they have the need to improve such materials, either through maintenance or partial replacement. Some methods to protect substrates from hot corrosion are pack cementations, chromising or deposition of silicon, aluminium and ceramic coatings among others. Substrates such as stainless steels, medium-high carbon steel and low alloy steels such as alloy T22 have been used in the application of methods for modifying their surface [1,7,16,18–20]. Alloy T22 is often required to operate in high temperature aggressive environments in superheaters of boilers, however due to its low corrosion resistance, it has been used as substrate for the application of metallic coatings [21]. From these investigations, coatings were found to be effective in reducing the overall corrosion with respect to bare T22. Therefore the aim of this paper is to evaluate the

CONTACT Cecilia Cuevas Arteaga ccuevas@uaem.mx

aggressiveness of a mixture V_2O_5-Na_2SO_4, highly recognised as responsible for fireside corrosion of the components of boilers of power generation plants [22], exposing the SS-HP40 with 26 wt.% Cr and the carbon steel T22 (CS-T22) with only 2.5 wt.% of chromium, determining the corrosion resistance of both materials. In this study, the traditional mass loss method and electrochemical techniques were applied, the last ones due to offer greater speed and sensitivity, which provide corrosion information based on the movement of charges at the interface between the corroding metal and the electrolyte. On the other hand, using electrochemical techniques such as Electrochemical Noise (EN), it is possible to measure instantaneous corrosion rates with any perturbations, whereas the measurements are done at open circuit potential (E_{OCP}) obtaining information about the kinetics and mechanism for metallic corrosion. The random current and potential noise signals emanating from the corrosion system can be used to determine the corrosion rate, while corrosion mechanism can be predicted based on the interpretation of the spectral noise signals and the so-called localisation index. From the EN, the resistance noise (R_n) can also be reported and utilised in order to obtain the corrosion rate. The ASTM G199 (2014) [23] which is a guide for Electrochemical Noise measurements was used as a reference, being extended for conducting EN measurements both in the laboratory and in service environments [24,25]. In addition this technique has been widely used in molten salts at high temperature [26–28]. The potentiodynamic polarisation curves (PC), which is the other electrochemical technique used in this research, can determine instantaneous corrosion current density (corrosion rate) when potential-current curves are analysed at the E_{OCP} within the so-called Tafel region. For the above, the electrochemical noise technique and the potentiodynamic polarisations curves (PC) were used and compared to the mass loss method results during 5 days. Images of the corroded samples from the scanning electron microscopy (SEM) helped to determine the type of corrosion suffered by both alloys, whereas the mappings of the main elements of the systems supported the corrosion mechanism developed by the two studied alloys. The physical characteristics of the corroded alloys together with the electrochemical results provided information to complement each other in order to analyse the corrosion performance of the studied materials.

Experimental procedure

Working electrodes

Specimens were made from a bar of HP40 and T22, which was cut into small rectangular parallelepipeds sized 10x5x2 mm, ground to 600 grit silicon carbide paper, rinsed with distiled water and degreased with acetone. The nominal composition of the SS-HP40 is: 0.55 C-2.0Mn-2.5Si-0.04P-0.04S-26Cr-35Ni-0.5Mo-Bal Fe [29] and for the CS-T22 (ASTM A213 grade T22): 0.09 C-0.45Mn-0.5(max)Si-0.025(max)P-0.025(max)S-2.25Cr-1.0Mo-Bal Fe. These samples were the working electrodes to which one 80% (wt.) Cr-20Ni wire (150 mm long and 1.0 mm in diameter) was spot welded [30–32]. For isolating the 80Cr-20Ni wire from the molten salt, ceramic tubes were used filling the gap between the ceramic tube and the electrical wire with refractory cement. The amount of corrosive mixture in each experiment was 2 g/cm^2, which was introduced into a 20 ml silica crucible. Then the silica crucible was set inside an electrical tube furnace to reach the test temperatures, which were 550°C and 650°C. The corrosive salt was prepared with analytical reagents at a concentration of 80 mol % V_2O_5-20Na_2SO_4.

Electrochemical techniques

For EN, the electrochemical cell was a three-electrode setup including two identical working electrodes (WE1 and WE2) and 1 mm diameter/150 mm long platinum wire as the reference electrode, which is a zero-resistance electrode [33–36]. Whereby the electrochemical potential and current noise were concurrently measured with great reliability, enabling the direct determination of the electrochemical noise resistance Rn [37], thus the corrosion rates over 120 hours were obtained and compared to the results from the conventional mass loss method. This electrode arrangement has been used under similar molten salt conditions [30,38,39]. For potentiodynamic polarisation curves, the electrochemical cell was constituted by the working electrode and two 1 mm diameter/150 mm long platinum wires as auxiliary and reference electrodes [30–32], which were also introduced in a ceramic tube sealing the gaps with refractory cement. Once the silica crucible containing the molten salt was set inside the electrical tube furnace and the test temperature was reached, the electrochemical cell was introduced inside the crucible and the corresponding cables of the potentiostat were connected to the electrochemical cell. In order to establish the steady state of the electrochemical system, the PC started 50 minutes after the test temperature was reached. Polarisation curves were accomplished potentiodynamically polarising the specimen at ±250 mV with respect to the corrosion potential at a scan rate of 1 mV/s, such as it has been reported elsewhere [33,40–43]. This over-potential was used to obtain the lineal portion of the polarisation curve in order to apply the Tafel extrapolation method, obtaining the Tafel slopes, the corrosion potential E_{corr} and the corrosion current density I_{corr}. Applying this over-potential is possible to avoid significant modifications of the metallic surface, which

may enhance the formation of metallic oxides on the corroding surface or produce the preferential dissolution of one element of the alloy, generating inaccuracy results as well as potential drops due to the pass of current through the electrical resistance of the electrolyte.

The simultaneous electrochemical current and potential noise and PC were carried out through an ACM Gill 8AC, which has integrated a zero-resistance ammeter (ZRA) coupled to a personal computer. The electrochemical noise data were recorded with a sampling frequency of 1 Hz; 1024 measurements were obtained each three hours during 5 days of immersion. Current and potential time series were analysed in the time and frequency domain to determine the corrosion activity and mechanism. A statistical analysis was made to the noise data for determining the resistance noise (Rn) and the localisation index (LI) [44]. The corrosion rates were determined from the Rn once applying the Stern-Geary equation and the Faraday´s Law. The spectral noise impedance plots for both alloys were obtained using an algorithm based on the Fast Fourier Transform (FFT) of the spectral analysis, which was resolved in a frequency bandwidth of interest between 0.5 Hz and 500 mHz. The working electrode used as WE1 was mounted (without descaling) in Bakelite and metallographically polished, then the cross-section was analysed by SEM to investigate the morphology and distribution of reaction products. X-ray mappings and microprobe analyses were carried out using a Microspec WDX-3PC system connected to a Zeiss DSM960 SEM.

Mass loss measurements

The mass-loss measurements were taken each 24 h during 5 days under the same conditions as that of the EN technique and were carried out according to ASTM Standards G1 and G31 [45,46] using specimens of duplicates of the same size as those used for EN. A total of 10 samples were utilised (two of them each day), which were totally packed in the corrosive salt contained in independent 20 ml silica crucibles. Every 24 h, two samples were removed from the muffle and the corrosion products of the samples were mechanically eliminated using alternating an ultrasonic bath during 5 cycles. After cleaning the samples in each cycle, these were weighted using an analytical and digital balance with a precision of 0.0001 g. The surface morphology of the clean corroded samples was obtained from SEM, whereas DXR analyses were made for the corrosion products obtained from the cleaning of the samples by means of a diffractometer operating with Cu Kα radiation, whose results were interpreted using the Powder Diffraction Data File [47]. The loss mass obtained each day during the immersion time from the conventional ML method was compared to the corrosion rates from R_n.

RESULTS AND DISCUSSION

Physical characterisation

Figure 1 presents images of corroded T22 and HP40 alloys exposed to 80 mol% V_2O_5-20Na_2SO_4 at 550°C obtained from the ML after being mechanically cleaned. From the images at 30x, it can be observed that the alloys suffered pitting corrosion, noting a major pitting density over the T22 surface. The corroded zones in both materials are sized in the range of 5–340 μm, observing that the pits of HP40 are the smallest ones. The anodic and cathodic areas are clearly seen in both materials. Adherent corrosion products are observed inside the pits in both materials, stating that the mechanical and ultrasound cleaning methods were not enough to eliminate all the corrosion products in the deepest sites of the pits. From the images at 500x, the biggest pit showed over the T22 surface seems to be an individual pit because of its circular shape, whereas the biggest pit of HP40, elongated with an irregular shape, seems to be made with the unification of several pits, which collapsed to form a bigger corroded area. With respect to HP40, some other small corroded sites seem to be also elongated and formed from other smaller pits. Some other many small and medium size individual pits together with their cathodic zones around them are observed too.

Images of both materials exposed at 650°C are shown in Figure 2. The presence of exacerbated pits is evident in both alloys, nevertheless alloy T22 shows bigger pits. In addition, T22 also shows several small and individual 20–40 μm diameter pits. From the HP40 images, dark and clear areas are seen, both presenting small and medium size 8–32 μm diameter pits. It is clear that the increment in temperature leads to intensify the size of pits together with the pitting density in both materials.

Cross-section images of the corroded T22 and HP40 at 550°C and 650°C were obtained together with X-ray mappings of the main elements composing the corrosive systems, nevertheless due to the behaviour was similar at both temperatures, in this work the X-ray mappings at 650°C are only presented, since the corrosion mechanisms at both temperatures were similar. Figure 3 shows a cross-section image of the corroded T22 exposed to 80 mol% V_2O_5-20Na_2SO_4 at 650°C together with the mappings of Cr, Fe, O and V. The mapping of Cr together with oxygen shows the development of a small concentration of Cr_2O_3 in the corrosion products zone together with Fe_2O_3, the last one being the major phase such as it has been reported by R. Kumar et al. [48] when exposed T22 at a molten salt Na_2SO_4-60% V_2O_5 at 900°C. The low

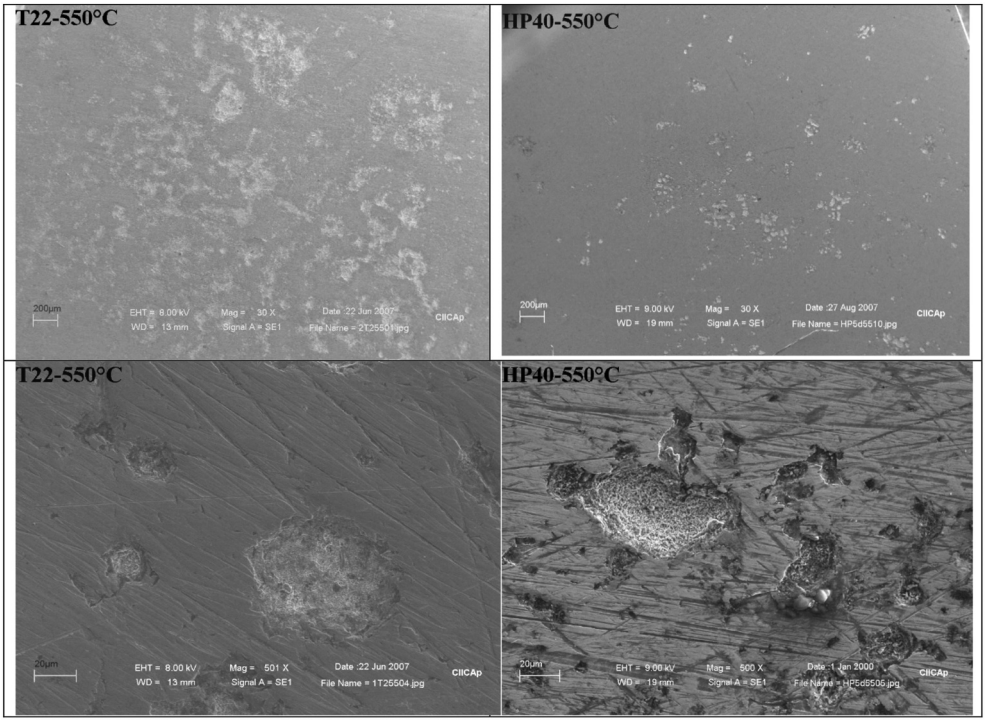

Figure 1. Corroded images of T22 and HP40 alloys exposed to 80 mol % V_2O_5-20Na_2SO_4 molten salt at 550°C after 5 days of exposure.

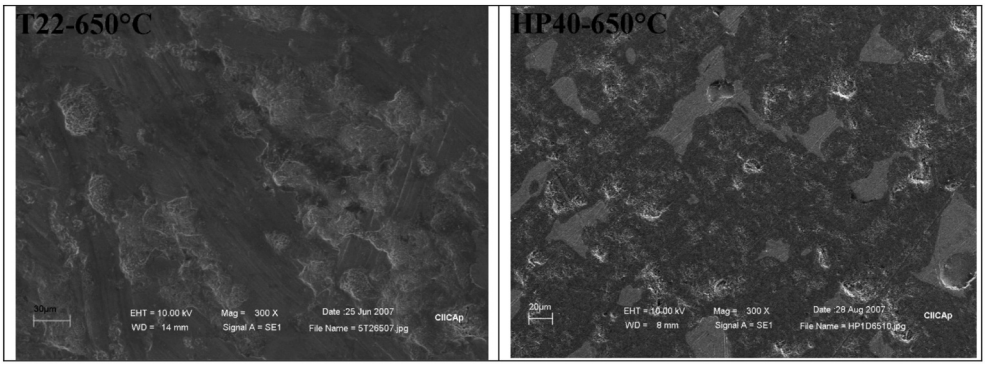

Figure 2. Corroded images of T22 and HP40 alloys exposed to 80% mol V_2O_5-20Na_2SO_4 molten salt at 650°C after 5 days of exposure.

concentration of Cr makes Fe vulnerable to preferential oxidation. Fluxing of the initial Fe-oxide leads to the attack of the base metal that is slightly enriched with Cr, creating a better defined intercalated appearance in the X-ray maps. Both oxides have been dissolved (especially the iron oxide) due to chemical interaction between the molten salt along the exposure. The mapping of oxygen shows a high concentration, evidencing the formation of the two metallic oxides, nevertheless the dense layer with a thickness of ≈ 65 μm formed on the metallic surface did not have an effective protection on suppressing further penetration of the molten salt. From the mapping of vanadium, it can be observed that this element is present in combination with the metallic oxides and oxygen, so it is highly expected that some V-O-metal ions compounds can form secondary corrosion products. The presence of V over the T22 surface together with the fact that T22 suffered pitting corrosion lead to consider that the metallic oxides were enough porous in order to permit that the corrosion species diffuse to the metal surface. In addition and in contrast to the mapping of oxygen, vanadium is part of the flux that attacks pseudo-protective oxides, therefore, it is possible the diffusion of vanadium until the deepest sites of the pits, stating that T22 presented very low corrosion resistance to high temperatures due to the low Cr and Si content [4].

Figure 4 shows a cross-section image of the corroded HP40 exposed to 80 mol % V_2O_5-20Na_2SO_4 at 650°C together with the mappings of Cr, Fe, Ni, O and V. From the micrograph, the metal-corrosion products interface can be seen. The mapping of Cr seems to be denser than that of Fe, even though

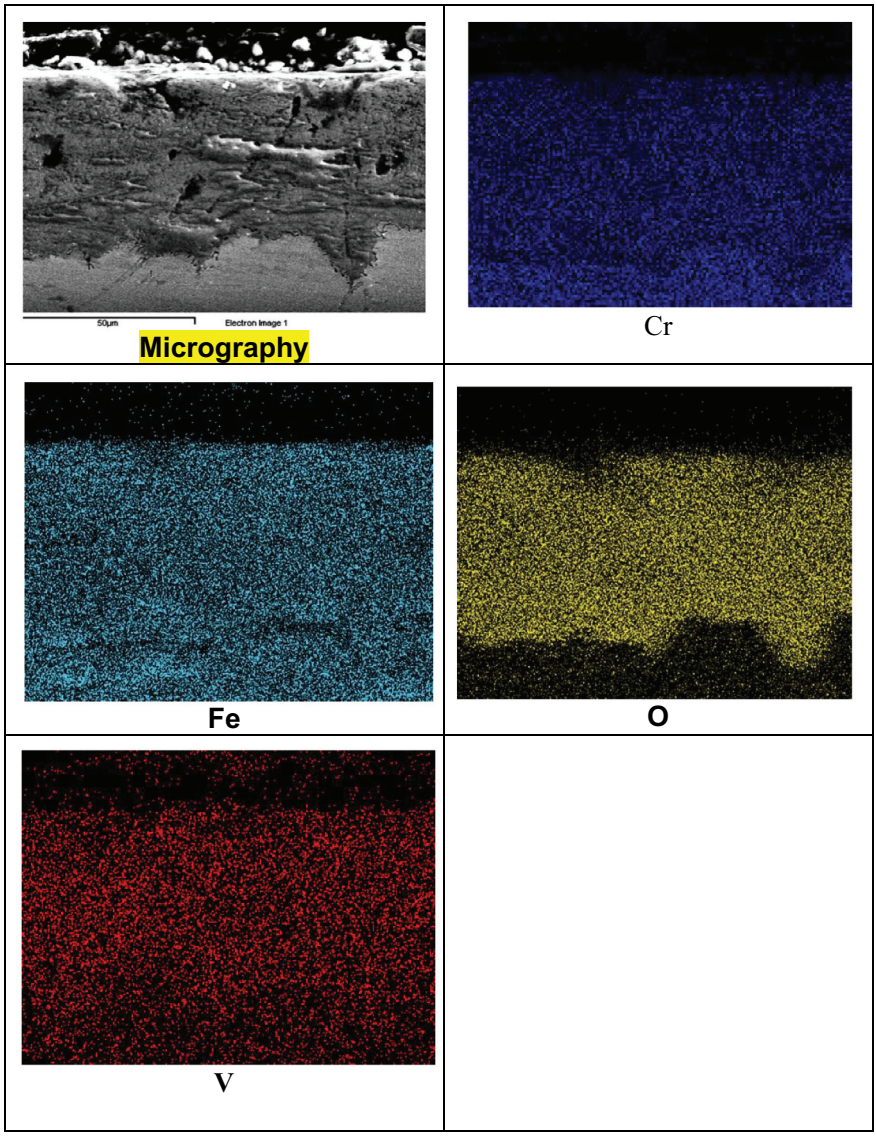

Figure 3. Electron image of the metal-scale interface and X-ray mappings of Cr, Fe, O and V of T22 exposed to 80 mol % V_2O_5-20Na_2SO_4 at 650°C.

through the Cr layer some free of chromium areas appear. Below the metal-scale interface, a depletion of chromium inside the substrate is seen. Cr in both materials is shown to be part of intercalated oxides, typical of acidic fluxing, which prevails in vanadium containing molten salts. The intercalated layering as indicated in the X-ray maps for Cr is more compliant with the initial formation of chromia for the HP40 followed by the subsequent dissolution by acid fluxing allowing for the formation of Fe-oxides. In addition, the iron-scale appears more homogeneous but with lower density, observing a stripe above the metal-scale interface with even lower concentration. Due to the large content of nickel in HP40, the mapping shows an important concentration of this element in the corrosion products layer, observing a major concentration just below the metal-scale interface inside the substrate. The intensity concentration of Ni is observed because Fe and Cr are depleted. In addition, the mappings of Ni and Fe presented a decrease in concentration over the metal surface, which is due to their dissolution by the high vanadium flux. Observing the mapping for vanadium, it is possible to determine that such low concentration presented by the Ni and Fe above the metal-scale interface is occupied by V, which is in combination with oxygen and chromium, this fact could allow us to elucidate the possible formation of vanadyl vanadates compounds, which will be confirmed from the DRX analyses of the corrosion products. The presence of 26% wt. of chromium in the alloy HP40 should increase the corrosion resistance of this material [49], nevertheless, accordingly to the morphological characterisation, alloy HP40 suffered a pitting corrosion process similar to alloy T22, but in a less intense way. Nickel in high concentration contributes to improve the mechanical resistance, however when iron base alloys containing chromium and nickel are exposed to sulphate-vanadium melting salts, a thin nickel oxide underneath the chromium and iron oxide is formed for protecting the alloy from

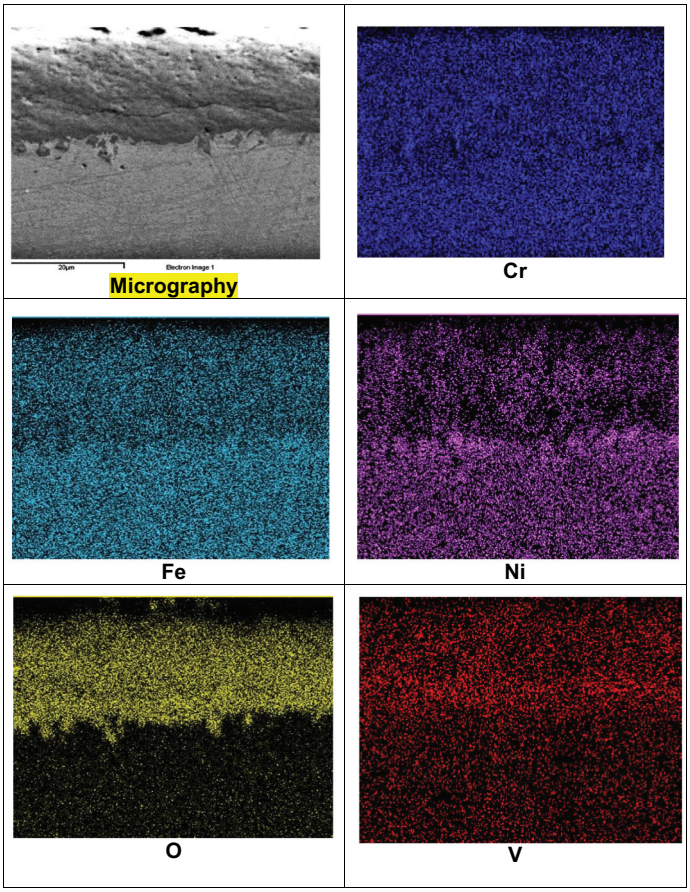

Figure 4. Electron image of the metal-scale interface and X-ray mappings of Cr, Fe, O and V of HP40 exposed to 80 mol % V_2O_5-20Na_2SO_4 at 650°C.

the diffusion of vanadium and sulphur [13,30,50]. In the particular case of HP40 under the experimental conditions of this work, nickel oxide layer was unprotective.

Figure 5 shows the XRD results of the corrosion products generated when T22 (6.a) and HP40 (6.b) were exposed at 650°C in the molten salt. According to the spectrum of the T22 alloy, Fe and Cr oxides were found in the corrosion products. Other compounds such as sodium vanadyl vanadates were obtained: $Na_2O.V2O_4.5V_2O_5$ (p.f. 550°C), $5Na_2O.V_2O_4.11V_2O_5$ (p.f. 535°C), $Na_8V_{24}O_{63}$ and NaV_2O_8 [3,48,51]. The presence of 1.1.5 and 5.1.11 vanadyl vanadates have been reported as especially corrosive due to V^{4+} and V^{5+} couple facilitates the oxygen transport through the melt generating major oxidation of the metal and exacerbating the corrosion rates [52].

The presence of Na-V-O compounds is in agreement with those compounds identified in some reported works under similar experimental conditions [4,22,38,53]. Furthermore, vanadates are able to dissolve selectively some metallic oxides normally protective, exposing metallic surface for further internal degradation. The $Na_8V_{24}O_{63}$ compound has been detected when the 80 (wt. %) V_2O_5-20Na_2SO_4 molten salt is exposed to temperatures higher than 600°C [54]. The formation of pits indicates that the initially formed Fe_2O_3 and Cr_2O_3 could perform as passive films at the beginning of the exposure, but then suffered an acid fluxing leading to the nucleation of pits as reported by R. Kumar under a similar mixture of salt at 900°C [48]. The corrosion products of HP40 were the same vanadyl vanadates with the exception of the 5.1.11. The metallic oxides formed over the HP40 surface were the iron and chromium together with a spinel composed of nickel and iron.

Electrochemical characterisation

Potentiodynamic Polarisation Curves

The PC of alloys T22 and HP40 at both temperatures are presented in Figure 6. The Tafel parameters were obtained applying the Tafel extrapolation method through the software of the potentiostat, which is a sophisticated instrumentation that operates on well-established theoretical basis to provide accurate corrosion information. The corrosion potential of alloy T22 resulted slightly more active with temperature, whereas the corrosion current density (i_{corr}) was an order of magnitude higher: 5.4 mA cm^{-2} at 550°C and 22.0 mA cm^{-2} at 650°C. In the case of HP40 the corrosion potential at 550°C was the noblest one (44 mV) evidencing that HP40 exposed to the lower

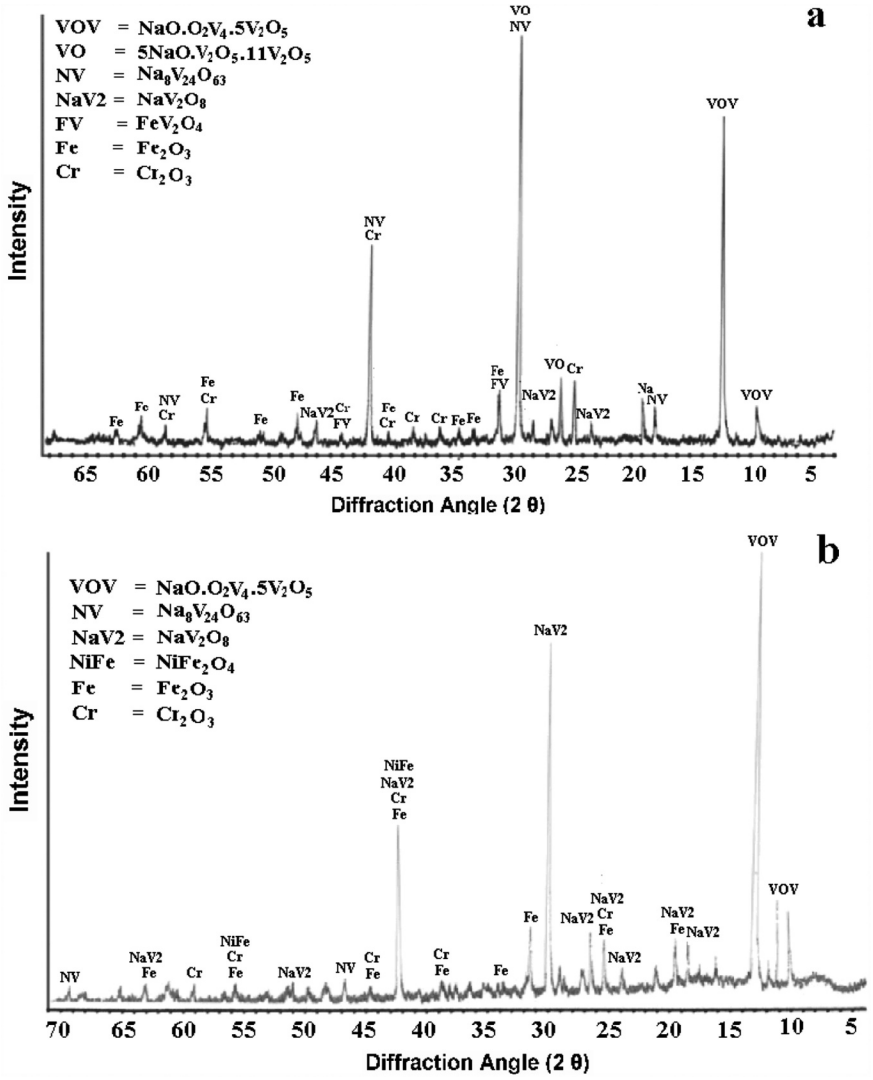

Figure 5. X-Ray diffraction results of T22 (a) and HP40 (b) exposed to 80 mol % V_2O_5-20Na_2SO_4 at 650°C.

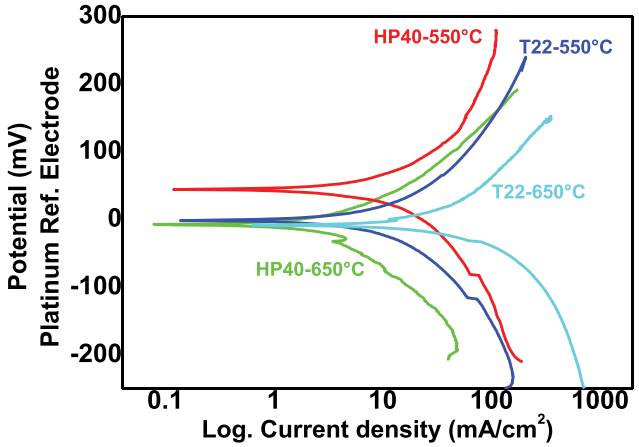

Figure 6. Potentiodynamic polarisation curves for alloys T22 and HK-40 m exposed to 80 mol% Na_2SO_4–20 mol% V_2O_5 at 550 and 650°C.

temperature presented a minor degradation such as the morphological characterisation indicated. With temperature, HP40 had a decrease in its corrosion potential showing to be more active to corrosion (−8 mV). The i_{corr} for the alloy HP40 is alike at both temperatures, thus the effect of the temperature on the corrosion process was from the thermodynamic point of view. The Tafel slopes are necessary because the anodic and cathodic slopes were used to determine the corrosion rates from the electrochemical noise data through the resistance noise R_n, applying the Stearn-Geary equation. The Tafel regions of the polarisation

curves for both alloys are similar and close to 100 mV dec^{-1}, except the anodic slope of alloy T22 exposed at 550°C, which is higher than the rest ones, hence they are well defined, demonstrating that the electron transfer is mostly significant during the degradation, specially for the alloy HP40, being the charge transfer process the rate controlling step [55,56]. For T22 exposed at 550°C, it is necessary to indicate that it is a typical system which is not purely activation or diffusion controlled.

Electrochemical Noise Measurements

The current and potential time series (CPts) and the spectral analysis (EAn) for alloy T22 at 550°C and 650°C are shown in Figure 7. To analyse the electrochemical noise pattern, the three typical forms of electrochemical noise generated by different types of corrosion processes were taken into account [57]: i) Type I (Pitting) consists of fluctuations of high amplitude with a high repetition rate; ii) Type II (Mixed) is a combination of transients of type I and oscillations of short amplitude; iii) Type III (Uniform) is formed by oscillations of low amplitude. It is feasible to observe several transients and random oscillations of low amplitude at both temperatures, evidencing a mixed corrosion process [58,59]. The current pattern at 650°C shows the presence of several higher amplitude transients with respect to that at 550°C, indicating a significant increase in current due to the breaking of the protective film that provoked a major oxidation of the material at a local site leading to the nucleation and/or the formation of pits [39,60]. The presence of a

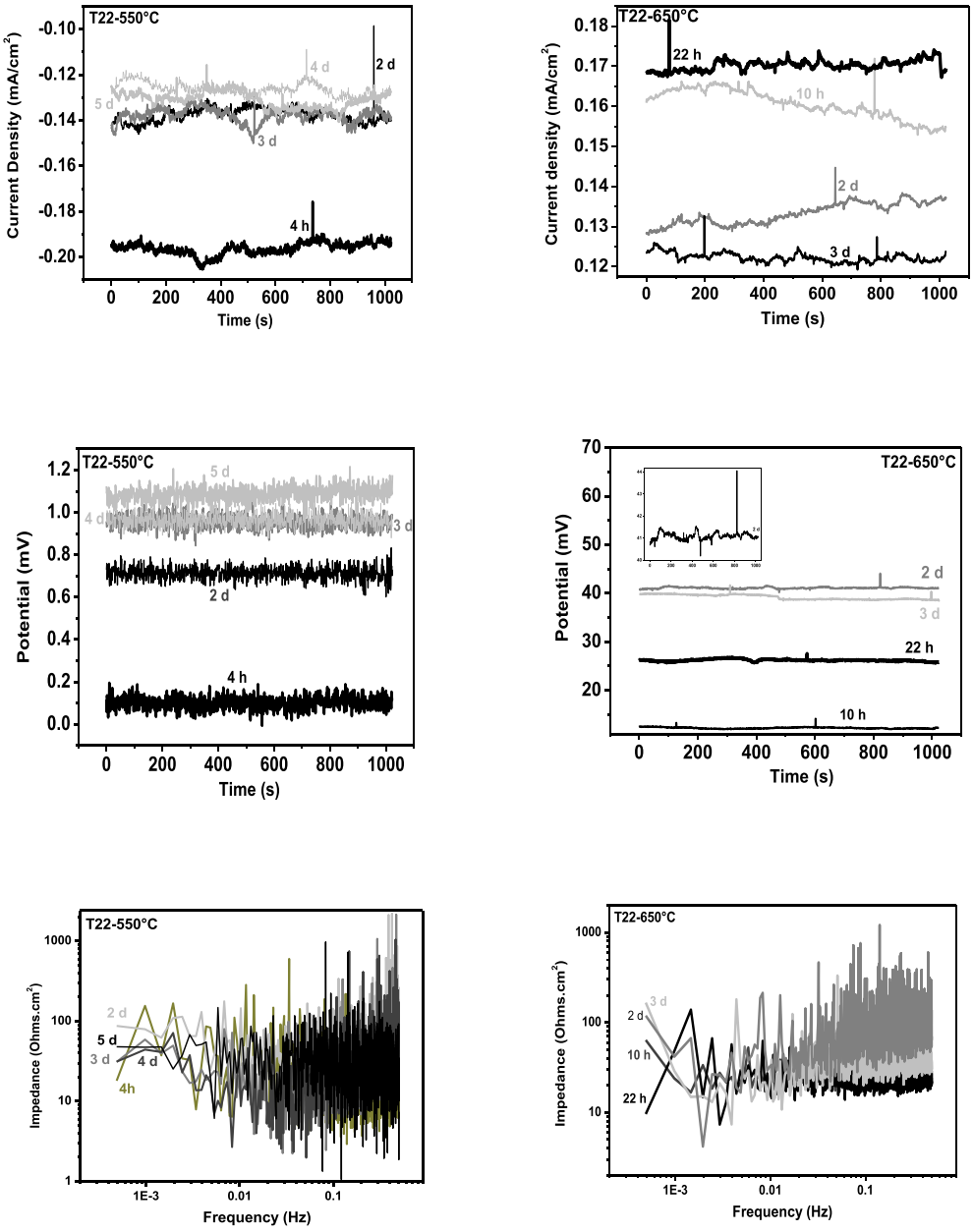

Figure 7. Time series of the electrochemical current and potential noise and the spectral analysis for alloy T22 exposed to 80% mol V_2O_5-20Na_2SO_4 molten salt at 550 and 650°C.

major number and more intense transients at 650°C reflects the presence of a major amount of pits, such as was evidenced through the physical characterisation.

The current density at 550°C is negative and at 650°C is positive, indicating the preferential dissolution of one of the two identical working electrodes [58]. In addition, the current densities have similar values at both temperatures; hence the corrosion behaviour is determined by the intensity of the transients, but especially by the propagation of transients. According to the mappings analyses, it presumes that the first stage of the corrosion process was the formation of an iron oxide layer accompanied by a Cr_2O_3 layer, which were initially protective, nevertheless, the local dissolution of such layers propitiated the nucleation of pits and then their propagation along the metallic surface. The exacerbation of the localised corrosion with temperature is evident accordingly to the images at 650°C (Figure 2). With respect to the potential noise pattern at 550°C, only white noise in a very small interval in potential (1 mV) is seen, whereas at 650°C the interval was of 33 mV with nobler potential values and some positive and negative transients, thus the corrosion activity was defined by the current pattern behaviour, which is in accordance with the PCs that showed few thermodynamic effects, since the corrosion potential was alike. The positive transients indicate the attempt of alloy T22 to passivate, whereas the negative ones indicate the propagation of pits [61]. The spectral analysis of alloy T22 at 550°C shows an oscillatory behaviour at low frequencies, starting with a low impedance and medium values at the end of the exposure. The average of the first 10 values of the impedance in Ohms.cm^2 was: 58.5, 83.6, 31.2, 32.8 and 48.1 at 4 h, 2d, 3d, 4d and 5d respectively. Such results show the physical condition of the metallic oxides, which until the second day showed a good protectiveness, then during the third and fourth days the metallic oxides suffered dissolution, which is confirmed by the great amount of vanadium in mixture with Fe, Cr and O showed through the mappings. At 650°C, the impedance values are similar to that at 550°C, being the impedance in both cases independent of the frequency.

Figure 8 shows the CPts together with the SAn for alloy HP40 exposed to 80% mol V_2O_5-20 % mol Na_2SO_4 molten salt at 550°C and 650°C. One of the features of the current time series at both temperatures is that the corrosion current density is one order of magnitude lower than that of the alloy T22, and the values at 550°C are smaller than that at 650°C, evidencing the major corrosion resistance of alloy HP40 with respect to T22 and the effect of corrosion activity when temperature increases. The current noise pattern of alloy HP40 has many positive transients of low intensity at 550°C, which is due to the pits were smaller than that for alloy T22. At 650°C the current time series show repetitively negative small transients, especially at the last two days, indicating the trend of HP40 to passivate, nevertheless, being the transients of low intensity, it seems to be that the recuperation of the initially protective metallic oxide was not possible, therefore the material cedes to the corrosion processes presenting a pitting corrosion type [62], being in congruence with the physical characterisation.

The spectral noise impedance at 550°C showed that the amplitude impedance was decreasing in time at low frequencies until the end of the experiment. The spectral noise impedance was in general independent of frequency and the magnitude of the noise impedance along the bandwidth was from 1 to 7200 ohms.cm^2. The average of the first 10 values at the lowest frequencies was 220, 22, 30 and 11 ohms.cm^2 at 2, 3, 4 and 5 d respectively, suggesting a deterioration of the initially formed passive layer of Cr_2O_3 by the effect of the aggressiveness of the high vanadium molten salt, so the nucleation of pits and their propagation could be seen over the corroded sample (Figure 1). The spectral noise at 650°C is observed between a narrow interval of impedance, from 0.4 to 5000 ohms.cm^2, and the average of the first 10 values at the lowest frequencies was 10.5, 23.6, 72.6 and 84.3 ohms.cm^2 showing a small increase in the corrosion resistance of the metallic oxides in time, which was not enough in order to mitigate the formation of pits.

Localisation Index

To corroborate the behaviour of the EN signals with respect to the type of corrosion, the localisation index (LI) was calculated as the ratio between the current noise standard deviation σ_i over the root-mean-square current value I_{rms} [57,63], which is an indicator of localised corrosion (LC). The analysis took into account the different ranges of LI values, which lie between 0 and 1 (See Figure 9) [64,65]. LI values were calculated from every one of the time series records obtained from the EN measurements. LI is similar for alloy T22 at both temperatures keeping in the localised and mixed corrosion zones. LI was mostly lower at 550°C along the exposure time, therefore the effect of temperature is decisive in the exacerbation of the LC. With respect to LI for alloy HP40 at 550°C, at the beginning of the exposure, LI maintained in the pitting corrosion zone, reaching the mixed corrosion zone from 12 h to 2.5 d, after that LI decreased until the uniform corrosion zone continuing in this zone until the end of the exposure. The images of the corroded HP40 showed the presence of several small pits, but a uniform corrosion process could be seen along a large area, demonstrating that LI parameter reflects the corrosion activity developed by the alloy HP40 when exposed to 550°C. At 650°C, LI followed almost the same behaviour as that at 550°C until 1.8 d, after that LI remained in the mixed

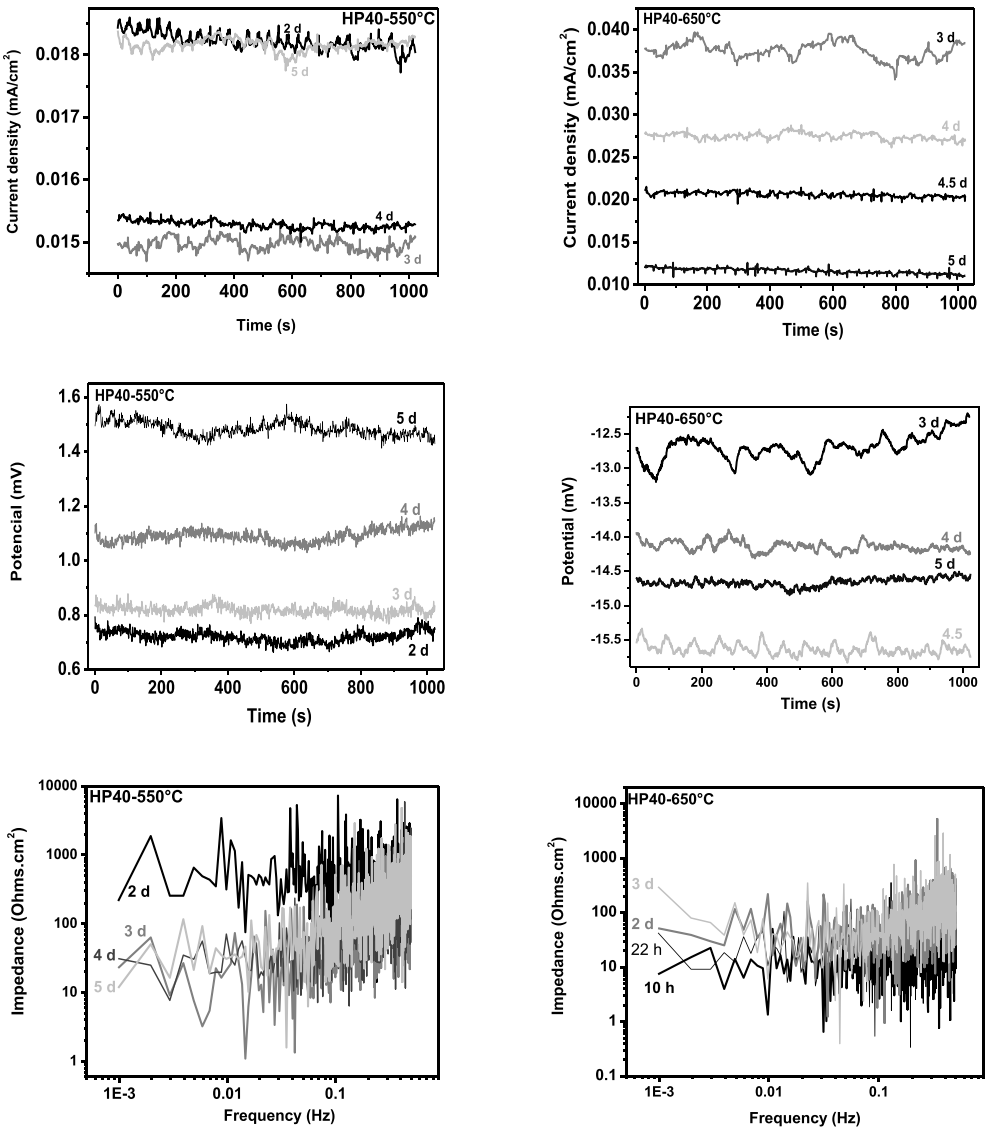

Figure 8. Time series of the electrochemical current and potential noise and the spectral analysis for alloy HP40 exposed to 80% mol V_2O_5-20Na_2SO_4 molten salt at 550 and 650°C.

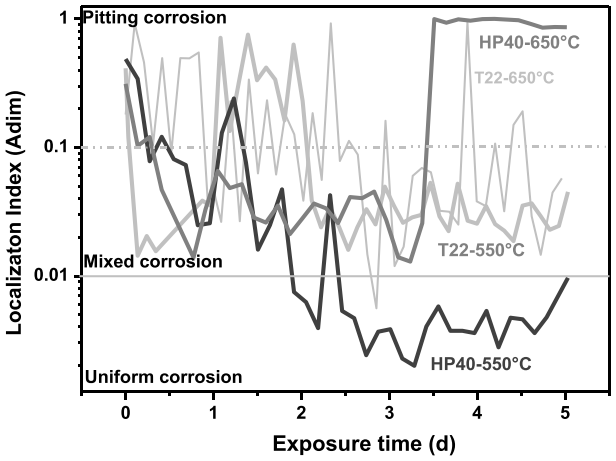

Figure 9. Localisation index of the corrosion process for alloys T22 and HP40 exposed to 80% mol V_2O_5-20Na_2SO_4 molten salt at 550 and 650°C.

corrosion zone until 3.5 d, after that, LI increased significantly until reaching the pitting corrosion zone, which is reflected over the metallic surface where a great amount of pits is found (see Figure 2). In conclusion and accordingly to the physical characterisation, LI parameter can be considered as an indicator of the prevailing corrosion mechanism of alloys T22 and HP40 [63].

Corrosion rates from EN and WLM

Figure 10 shows the experimental corrosion rates in time obtained from the EN and the ML methods for alloys T22 and HP40 exposed to 80 mol% V_2O_5-20Na_2SO_4 at 550°C and 650°C. To determine the mass loss in time the noise resistance R_n (evaluated as the ratio of the potential noise standard deviation over the current noise standard deviation) was calculated [63–65]. Approximately 40 R_n data during 5 days of exposure were obtained. R_n (ohms.cm^2) data were used in the Stern-Geary equation to obtain the corrosion current density I_{corr} (mA.cm^{-2}), then the Faraday Law [60,66–68] was utilised to obtain the mass loss, as

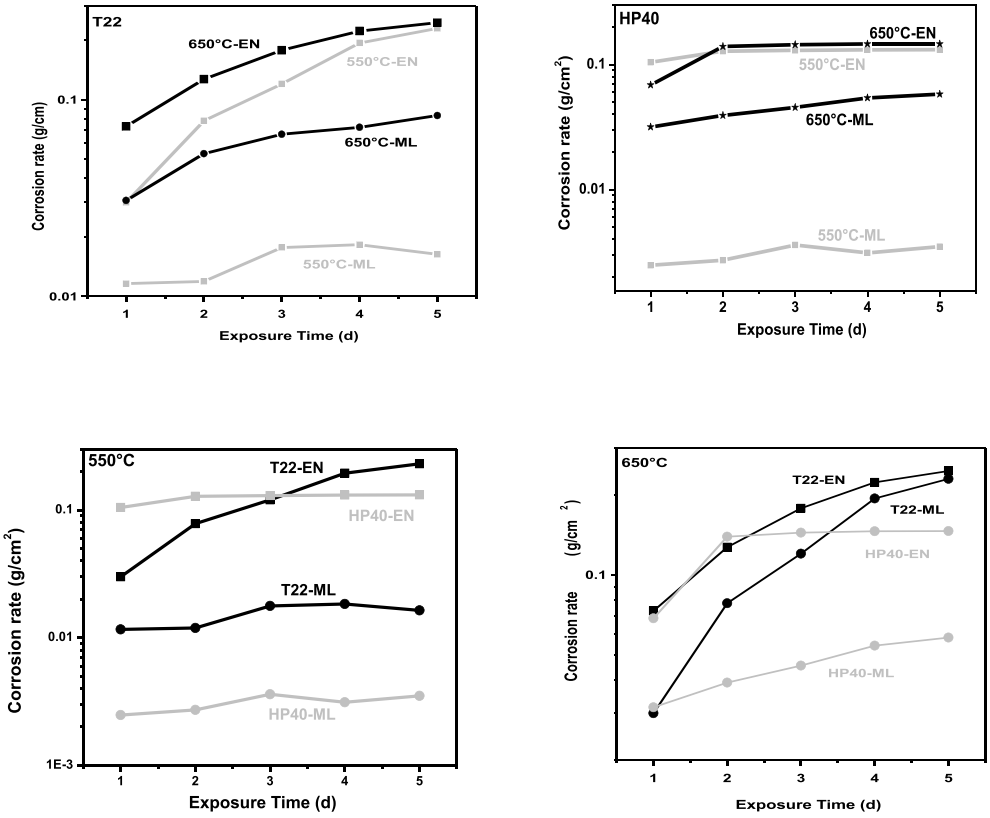

Figure 10. Cumulative mass loss for alloys T22 and HP40 exposed to 80% mol V_2O_5-20Na_2SO_4 molten salt at 550 and 650°C obtained from the electrochemical noise data and the conventional mass loss method.

described elsewhere [69,70]. To calculate the Tafel constant B of the Stern-Geary equation, Tafel slopes from the experimental PC were utilised (See Table 1). The behaviour of the corrosion kinetics showed that the corrosion rates obtained from EN are faintly higher than those obtained from ML for both materials, which may be due to a small amount of corrosion products are still adhered to the metallic surface of the corroded samples from the ML. In the case of alloy T22 the behaviour of the corrosion kinetics obtained from EN is increasing in time at both temperatures with a tendency to be constant at the last day of exposure, such tendency is similar to that from ML, except that at 550°C, whose corrosion rate decreased during the last day, showing the effect of temperature. From EN, the corrosion rate of HP40 at 650°C resulted slightly higher than that at 550°C keeping almost constant along the experimental time. At 650°C the corrosion rate from both techniques is very similar, not so at 550°C. The corrosion rate from both techniques is in the same order of magnitude, so that, it can be said that the results are comparable in magnitude. In general, the corrosion kinetics show that T22 degrades more than HP40, presenting certain differences in their behaviour. The corrosion rate of both materials from both techniques at 650°C behaves similar, especially for T22 whose values are very close.

Table 1. Parameters of the polarisation curves of T22 and HP40 at the test temperatures.

Material	Temperature [°C]	Icorr [mA cm^{-2}]	Ecorr [mV]	Ba [mV dec^{-1}]	Bc [mV dec^{-1}]
T22	550	5.4	−1.0	171.0	137.0
T22	650	22.0	−8.0	101.0	49.0
HP40	550	8.1	44.0	112.0	114.0
HP40	650	6.9	−8.0	138.0	117.0

Discussion

The corrosion process in molten salts at high temperature usually performs through three stages [3,51]: during the first one the materials form reaction products and a protective metallic oxides layer on the surface beneath the deposit, this layer is formed by the effect of the corrosive molten salt. This layer could be composed of one layer or multi-layers, which depends on the composition of the material. The second stage is performed when the oxide layers start to become porous layer due to the chemical interaction with the corrosive active species, then the oxide layer is no longer protective and molten salts reach the metal surface and the degradation of the material proceeds; in addition the depletion of chromium can be seen. The third stage consists in the propagation of a hot corrosion process (for instant pitting corrosion), and a scale far from the surface is formed with secondary compounds constituted by some elements of the material previously oxidised that are chemically complexed

with some elements or compounds from the corrosive molten salts. A fourth stage can be considered when a material starts to have a catastrophic failure. The propagation of an intensified stage for T22 was developed due to the increase in temperature, the high concentration of vanadium in the molten salt and for the porous and non-adherent metallic oxides of the alloy, whose composition was mainly iron. The diffusion of oxygen through the molten salt is an important aspect taken into account when the corrosion is being evaluated, especially for the initial hours of exposure [48,71]. The capability of alloys in withstanding the harsh environment of gas turbines, furnaces, boilers, etc., depends on their metallic oxides, whose properties must include a high density (no porous), adherence and high thickness [7]. The morphological analyses from SEM and DRX together with the electrochemical characterisation results and the conventional mass loss method of T22 alloy, allow to assume that this material formed two oxides, being the main one the F_2O_3 which presumably is present as a layer, followed by the formation of Cr_2O_3 in combination with the Fe_2O_3 (see the corresponding mappings), which were non-protective such as it has been reported by R.K.S. Raman [72]. Due to the large amount of Fe in the alloy T22, its corresponding non-protective iron oxide was dissolved forming a secondary compound as iron vanadate FeV_2O_4 accordingly to the DRX analyses of the corrosion products. In the case of alloy HP40, a main Cr_2O_3 layer accompanied by an iron and nickel layer was formed, the last two combined to form the spinel $NiFe_2O_4$ (Figure 5.b). The porosity of the initially passive layers generated due to the dissolution by the very oxidant vanadium species was evident, especially at the higher temperature where the pitting corrosion was exacerbated in both materials. The formation of some complex sodium vanadyl vanadates such as $Na_2O.V2O_4.5V_2O_5$, which melts at a relatively low temperature (550°C) is found to be the most common salt deposit on boiler superheaters, reducing the useful life of the components [3,56]. The fusion points of some sodium vanadyl vanadates are lower than the smallest temperature of this research, thus this fact provoked an increase in fluidity of the corrosive medium diminishing the viscosity of the molten salt. Such fluidity causes that the corrosive species can diffuse through the porous oxides and therefore reach the metallic surface in order to oxidise the alloying elements of the material in an accelerated and localised way.

The accelerated oxidation leads to the same type of corrosion for T22 and HP40, but in the case of alloy T22, pitting corrosion was more intensified generating higher corrosion rates at both temperatures. The dissolution of Fe_2O_3 and Cr_2O_3 of alloy T22 and Fe_2O_3, Cr_2O_3 and NiO of alloy HP40 was evident from their corresponding mappings and for the type of corrosion suffered for both materials. Clearly alloy T22 presented a major degradation due to iron is not recognised as a corrosion resistant element [73] and due to its low concentration of Cr. Nevertheless, even though HP40 contains an important amount of Cr, this material also suffered pitting corrosion of minor intensity, presenting lower pitting density and lower corrosion rates. This difference was due to Cr_2O_3 having a major growth rate, which leads to a more efficient protection and a rapid recuperation of the protective layer [74]. However, the corrosion rates of HP40 at both temperatures kept almost constant along the exposure time or with a tendency to be constant at the end of the 120 hours, which is in agreement with that reported by Zhang and Rapp [74,75], who suggested that the dissolution of chromia in the molten salt would lead to new compounds that neutralises the ionic character of the melt, resulting in a reduction of the corrosion rates as long as the Cr-saturated melt would be allowed to reside on the metal surface.

The fact that the potentiodynamic polarisation curves have a similar behaviour even though alloy HP40 has a nobler corrosion potential at 550°C and the alloy T22 developed a bigger corrosion current density at 650°C, and both materials suffered pitting corrosion despite having different alloying elements is due to the unique corrosive characteristics of the high vanadium molten salt, demonstrating that although an alloy owns good corrosion-resistant elements, the exposure in this molten salt can lead to a localised corrosion process. Therefore, it is confirmed that a strong acidic vanadium oxide [8,9,76] is able to produce pitting corrosion to high content chromium alloys.

Molten salts containing the transition vanadium species such as V^{+4} and V^{+5} are very oxidant and have the ability to absorb oxygen [5], which is another powerful oxidant that reduces forming oxygen ions, which react with metal cations in order to form protective metallic oxides leading to a passivation state or non-protective oxides [77]. Once the oxygen is absorbed, its transportation through the molten salt and the metallic oxide is very easy due to the high vanadium molten salt behaves as a semiconductor involving electron transfer, which facilities such transportation [73,78,79]. The facility of oxygen to be transported along with the vanadium species to the metal surface exerts a major rate of the oxidation reactions leading to a major corrosion rate with respect to other molten salts containing high sulphate compounds, whose corrosion processes are usually due to ionic diffusion [56,80]. By the other hand, the fact that high vanadium molten salt is an acidic mixture favours the major dissolution rate of any metallic oxide, since the solubility of all the metallic oxides increases, specially for the Cr_2O_3 more than that for

Fe_2O_3 and NiO_2 [5,10,64], so that, the diffusion of oxygen, vanadium or some vanadium compounds (which can be more aggressive than vanadium) could not be avoided [73]. The acidic dissolution rate can be so high that even materials composed of elements normally resistant could not be protective enough for the alloys resulting in the degradation of the materials at an unpredictable high corrosion rate or catastrophic failure [51]. Zhang and Rapp et al. [75] reported that every oxide should form an acidic solution with much higher solubility in the presence of vanadates, which should contribute to the more accelerated attack of oxides by mixed sulphate-vanadate melts than a pure sulphate melt. In addition, these new solutes added to the original molten salt and derivate from a fluxing process due to the dissolution of metallic oxides by the molten salt (which has been reported by other authors [2,79,81,82]) could control the corrosion behaviour, whose extent may be determined by the changes in the chemistry of the molten salt and the temperature rather than the materials selection. Therefore, the corrosion rate depends on the dissolution rate, which is higher in more complex low-melting point salts [5]. In the case of alloy HP40, which contains a great amount of chromium (26 wt.%) together with 2 wt.% of silicon, pitting corrosion was developed at both studied temperatures at less intensity with respect to alloy T22, which is mainly composed by iron (96 wt. %). Surface modifications to improve the corrosion resistance of low-cost alloys or alloys with no good alloying elements are an economical and attractive alternative instead of the expensive corrosion – resistant alloys. A low-grade steel surface modified by a suitable coating can provide good corrosion resistance similar to that obtained with an expensive superalloy [16,79,83].

Considering the types of high-temperature corrosion reported by some authors [5,51], the corrosion phenomenon observed in the present study involves the combination and sum of certain aspects of hot corrosion type *I* (TIHC) and type *II* (TIIHC), limited by some experimental parameters and control variables. This way, considering the above discussion, it is possible to describe the corrosion mechanisms of T22 and HP40 as next: The temperature range for TIIHC is 650–800°C (or as reported elsewhere below 750°C [4]), being the lower test temperature of this study 550°C, some aspects of this type of hot corrosion were observed for both materials at the two temperatures: i) a pitting corrosion was present due to the localised failure of the scale, ii) new corrosion reaction products were produced due to a fluxing dissolution and added to the molten salt changing the chemistry of the original salt. With respect to the TIHC, even when this type of corrosion is mainly seen in the temperature range of 825–950°C when the condensed phase is clearly liquid [4,5], some aspects of this type of corrosion were seen in the corrosion process of T22 and HP40 alloys: i) the attack of the oxide film to deplete the chromium from the substrate, ii) The broadening of the range of attack at the higher temperature, due to the formation of new solutes coming from the dissolution and fluxing of the metal oxides, iii) the presence of secondary vanadium compounds accelerates the corrosion rates, iv) the formation of extremely aggressive liquid phases of V formed at temperatures as low as 535°C, v) the increase in the solubility of the oxides due to the formation of vanadium compounds when the molten salt is a mixture of V_2O_5-Na_2SO_4.

Conclusions

According to the results, it can be concluded that alloy HP40 is slightly more resistant than the alloy T22 when exposed to the 80% mol V_2O_5-$20Na_2SO_4$ molten salt at 550 y 650°C, suffering both alloys a localised corrosion process. Nevertheless, it was observed that the amplitude of the current transients from the noise pattern was higher for T22, indicating that the depth and the density of the pits were bigger, which could be demonstrated through the images of the corroded samples. The corrosion rates plots showed that HP40 corroded with a smaller corrosion rate, observing that its behaviour was kept almost constant in time, as opposed to alloy T22, whose corrosion rate was increasing in time. The reason why alloy HP40 with large amount of one of the most corrosion resistant elements (26 wt.% Cr) suffered the same type of corrosion than alloy T22 whose content in Cr is considerably minor, is due to high vanadium molten salt is extremely oxidant and acidic, which results in accelerated oxidation and dissolution reactions, thus the passive layer breaks resulting in a type of pitting corrosion. Additionally, high vanadium molten salts have the ability to absorb oxygen and behave as semiconductors, which exacerbated the degradation of both materials.

Disclosure statement

No potential conflict of interest was reported by the authors.

Funding

This work was supported by the None [No applied].

ORCID

Christian Marisol Clemente http://orcid.org/0000-0003-2651-8863

References

[1] Mangla AK, Chawla V, Singh G, Review paper on high temperature corrosion and its control in coal fired boilers, international journal of latest trends in

engineering and technology, Special Issue AFTMME-2017, pp. 88–92.
[2] Rani A, Bala N, Gupta CM. Characterization and hot corrosion behavior of D-gun sprayed Cr 2O3-75% Al 2O3 coated ASTM-SA210-A1 boiler steel in molten salt environment. Anti-Corrosion Methods and Materials. 2017;64/5(5):515–528.
[3] Singh H, Puri D, Prakash S. An overview of Na_2SO_4 and/or V_2O_5 induced hot corrosion of Fe- and Ni-based superalloys. Rev. Adv. Mat. Sci.. 2007;16:27–50.
[4] Mahajan S, Chhibbe R. Hot corrosion studies of boiler steels exposed to different molten salt mixtures at 950°C. Eng Fail Anal. 2019;99:210–224.
[5] Salehi Doolabi M, Ghasemi B, Sadrnezhaad SK, et al. Hot corrosion behaviour and near-surface microstructure of a "low temperature high-activity Cr-aluminide" coating on inconel 738LC exposed to Na_2SO_4, Na_2SO_4+V_2O_5 and Na_2SO_4+V_2O_5+NaCl at 900 °C. Corros Sci. 2017;128:42–53.
[6] Guo L, Ch ZM, Sun LW, et al. Hot corrosion evaluation of Gd_2O_3-Yb_2O_3 co-doped Y_2O_3 stabilized ZrO_2 thermal barrier oxides exposed to Na_2SO_4+V_2O_5 molten salt. Ceram Int. 2017;43(2):2780–2785.
[7] Vakilifard H, Ghasemi R, Rahimipour M. Hot corrosion behaviour of plasma-sprayed functionally graded thermal barrier coatings in the presence of <sub>Na_2SO_4+ V_2O_5 molten salt. Surf Coat Technol. 2017;326:238–246.
[8] Guo L, Ch ZQ, Yu HJ, et al. Microstructure evolution and hot corrosion mechanisms of Ba_2REAlO_5 (RE=Yb, Er, Dy) exposed to V_2O_5+Na_2SO_4 molten salt. J Eur Ceram Soc. 2018;38(10):3555–3563.
[9] Ch ZL, Yu GJ, Ji V, et al. Hot corrosion behavior of Ba2REAlO5 (RE = Dy, Er, Yb) ceramics by vanadium pentoxide at 900–1000 °C. Ceram Int. 2017;43 (15):11944–11952.
[10] Rapp RA. Hot corrosion of materials. High Temperature Science. 1990;27:355–367.
[11] Viswanathan R, Sarver J, Tanzosh JM. Boiler Materials for Ultra-Supercritical Coal Power Plants —Steamside Oxidation. J Mater Eng Perform. 2006;15-3(3):255–274.
[12] Paul LD, Seeley RR, "Oil ash corrosion - A review of utility boiler experience", CORROSION/90 (NACE International), paper 267, pp. 267/1-15, (1990).
[13] Wong-Moreno A, Mujica Martínez Y, Martínez L, High temperature corrosion enhanced by residual fuel oil ash deposits, Corrosion/94 (NACE International), Paper 185, pp 185–1/185-13, (1994).
[14] Moosa AA. Oxidation properties of steel-T22 alloy coated by simultaneous ge-doped chromizing-siliconizing process. Eng.&Tech. 2008:26. https://www.researchgate.net/publication/238071095
[15] Hwang YS, Rapp RA. Thermochemistry and solubilities of oxides in sodium sulfate-vanadate solutions. Corrosion. 1989;45(11):933–937.
[16] Sotelo-Mazon O, Porcayo-Calderon J, Cuevas-Arteaga C, et al. Corrosion performance of Ni-Based Alloys in sodium metavanadate at 700 °C. Int. Journal of Electrochemical Science. 2016;11:1868–1882.
[17] Sidhu TS, Prakash S, Agrawal RD. Hot corrosion and performance of nickel-based coatings. Curr Sci. 2006;90-1:41–47.
[18] Sidhu TS, Prakash S, Agrawal RD. Studies on the properties of high-velocity oxy-fuel thermal spray coatings for higher temperature applications Mat. Sci. 2005;41-6:805–823.
[19] Sidhu HS, Sidhu BS, Prakash S. Evaluation of the hot corrosion behavior of LPG assisted HVOF NiCr wire sprayed boiler tube steels in molten salt environments. ISIJ Inter. 2006;46-7(7):1067–1074.
[20] Bala N, Singh H, Prakash S, et al. Investigations on the behavior of HVOF and cold sprayed Ni-20Cr Coating on T22 boiler steel in actual boiler environment. J Therm Spray Technol. 2012;21-1(1):144–158.
[21] Kumar S, Kumar M, Handa A. Combating hot corrosion of boiler tubes – A study. Eng Fail Anal. 2018;94:379–395.
[22] Amaya M, Espinosa-Medina MA, Porcayo-Calderon J, et al. High temperature corrosion performance of FeAl intermetallic alloys in molten salts. Mat Sci Eng. 2003;A349:12/19.
[23] The ASTM G199 (2014) Standard guide for electrochemical noise measurements.
[24] Seyed E, Jamali S, Mills DJ. A critical review of electrochemical noise measurement as a tool for evaluation of organic coatings. In: Australian institute for innovative materials – papers. University of Wollongong-Research Online; 2016.
[25] Obot IB, Onyeachu IB, Zeino A, et al. Electrochemical noise (EN) technique: review of recent practical applications to corrosion electrochemistry research. Journal of Adhesion Science and Technology. 2019;33-13(13):1453–1496.
[26] Frederik Vilhelm C, Niels B, Irina P. Electrochemical noise measurements of steel corrosion in the molten NaCl-K_2SO_4 system. J Electrochem Soc. 2005;152-7: B228–B235.
[27] Cutler AJB, Grant CJ. "Corrosion of iron and nickel base alloys in alkali sulphate melts", Proceedings of the international symposium on metal slag gas reactions and processes. Pub. The electrochemical society, Toronto Canada, pp.591–607, (1975).
[28] Grant CJ. Electrochemical corrosion measurements on In 738 and FSX 414 gas turbine alloys in molten sulphates. British Corrosion Journal. 1979;14(1):26–32. num
[29] ASTM Designation: A297/A297M–14, "Standard specification for steel castings, Iron -Chromium and Iron-Chromium-Nickel, heat resistant, for general application" 2017.
[30] Cuevas-Arteaga C, Uruchurtu U, González J, et al. Cano-Castillo, corrosion evaluation of alloy-800 in sulphate/vanadate molten salts. Corros Corros. 2004;60-6(6):548–560.
[31] Cuevas-Arteaga C, Uruchurtu-Chavarin J, Porcayo-Calderon J, et al. Study of molten salt corrosion of HK-40m alloy applying linear polarization resistance and conventional weight loss method techniques. Corr Sci. 2004;46-11(11):2663–2679.
[32] Cuevas-Arteaga C, Porcayo-Calderón J, Izquierdo G, et al. Study of hot corrosion of alloy800 using linear Polarization resistance and weight loss measurement. Mat. Sci. Technol. 2001;17(7):880–885.
[33] Almeraya F, Martínez-Villafañe A, Gaona C, et al. Corrosión por depósitos salinos de los aceros SA213-T22 y SA213-TP347H en presencia de una mezcla 80%V_2O_5-20%Na_2SO_4-20%Na_2SO_4. Rev. Metal Madrid. 1998;34-1(1):11–17.
[34] Martínez Villafañe A, Almeraya-Calderón F, Gaona Tiburcio C, et al. Evaluation of corrosion resistance of

two engineering alloys in molten salts by electrochemical techniques. Mater Corros. 2003;54(1):32–36.
[35] Salinas G, Gonzalez-Rodriguez JG, Porcayo-Calderon J, et al. Electrochemical study on effect of Au, Ag, Pd and Pt on corrosion behaviour of Fe3Al in molten NaCl–KCl. Corros Eng Sci Technol. 2014;49-5:379–385.
[36] Amin MA, Khaled KF, Fadl-Allah SA. Testing validity of the Tafel extrapolation method for monitoring corrosion of cold rolled steel in HCl solutions – experimental and theoretical studies. Corros Sci. 2010;52(1):140–151.
[37] Cottis RA. Sources of electrochemical noise in corroding systems. Russ J Electrochem. 2006;42(5):497–505.
[38] Gao G, Stott FH, Dawson JL, et al. Electrochemical monitoring of high-temperature molten salt corrosion, Oxid. Met. 1990;33:79–94.
[39] Farrell DM, Stott FH, Rocchini G, et al. Electrochemical aspects of high-temperature corrosion reactions in combustion systems. In: U.K. Corrosion 91. Vol. 2. Manchester: European Federation of Corrosion; 1991. p. 1–14.
[40] Poorqasemi E, Abootalebi O, Peikari M, et al. Investigating accuracy of the Tafel extrapolation method in HCl solutions. Corros Sci. 2009;51(5):1043–1054.
[41] Frangini S. Testing procedure to obtain reliable potentiodynamic polarization curves on type 310S stainless steel in alkali carbonate melts. Mater Corros. 2006;57-4(4):330–337.
[42] Zhang D1XL, Zh.H. J, Zh.P. Y, et al. Effects of scan rate on the potentiodynamic polarization curve obtained to determine the Tafel slopes and corrosion current density. Corros Sci. 2009;51(3):581–587.
[43] Singh E1IB. Corrosion and sulphate ion reduction studies on Ni and Pt surfaces in with and without V2O5 in (Li,Na,K)2SO4 melt. Corros Sci. 2003;45(10):2285–2292.
[44] Sanchez-Amaya JM, Cottis RA, botana FJ. Shot noise and statistical parameters for the estimation of corrosion mechanisms. Corros Sci. 2005;47-12(12):3280–3299.
[45] ASTM G1-03(2017) e1, Standard Practice for Preparing, Cleaning and Evaluating Corrosion Test Specimens.
[46] ASTM NACE/ASTMG31-12[a], Standard guide for laboratory immersion corrosion testing of metals, ASTM international, West Conshohocken, PA, 2012.
[47] Berry LG, Ed. Powder diffraction data file – inorganic phases, publication of the joint committee on powder diffraction standards. Swarthmore, PA: Centre for Diffraction Data.
[48] Kumar R, Tewari VK, Prakash S. Studies on hot corrosion of the microstructurally different regions of 2.25Cr-1Mo (T22) boiler tube steel weldment. J Mater Eng Perform. 2009;18(7):959–965.
[49] Birks N, Meier GH, Pettit FS. Introduction to the high temperature oxidation of metals. Cambridge University Press, Pittsburgh; 2012. 10.1017/CBO9781139163903
[50] Cho SH, Hur JM, Seo CS, et al. Hot corrosion behavior of Ni-base alloys in a molten salt under an oxidizing atmosphere. J Alloy Compd. 2009;468(1–2):263–269.
[51] Eliaz N, Shemesh G, Latanision RM. Hot corrosion in gas turbine components. Eng. Failure Analysis. 2002;9(1):31–43.
[52] Ramos-Hernandez JJ, Porcayo-Calderon J, Salinas-Bravo VM, et al. Phase stability diagrams for high temperature corrosion processes. Math. Prob. Eng. Vol.. Paper 542061. 2013;1–7.
[53] Alexander PA, Marsden RA. Corrosion of superheater materials by residual oil ash, International Conference on the mechanism of corrosion by fuel impurities. In: Wyatt LM, Evans GJ, editors. Butterworths. Marchwood; 1963. p. 542–555.
[54] Wong-Moreno A, Marchán Salgado RI, Martínez L, "Molten Salt Corrosion of heat resisting alloys", CORROSION/95 (NACE International), Paper 465, pp. 465/1-465/16, (1995).
[55] Skinner W. Influence of experimental inaccuracies on corrosion rates and Tafel slopes determined from electrochemical measurements in different overpotential ranges. Br. Corros. J. 1987. 1987;22-3(3):172–175.
[56] Cuevas-Arteaga C. Corrosion study of HK-40m alloy exposed to molten sulfate/vanadate mixtures using the electrochemical noise technique. Corros Sci. 2008;50(3):650–663.
[57] Alawadhi AA, Cottis RA, "Electrochemical noise signature analysis using power and cross-spectral densities", CORROSION/19990, (NACE-International), paper 207, pp. 207/1-207/24, (1999).
[58] Cottis R, Turgoose S. Electrochemical impedance and noise. In: Syrett BC, editor. NACE corrosion testing made easy. Houston: 1999.
[59] Breslin CB, Rudd AL. Activation of pure Al in an indium-containing electrolyte – an electrochemical noise and impedance study". Corros.Sci. 2000;42(6):1023–1039.
[60] Scully JR. Electrochemical, corrosion tests and standards: application and Interpretation. In: ASTM Manual Series: MNL. Vol. 20. Robert Baboian Press;1995.
[61] Cheng YF, Wilmott M, Luo JL. Analysis of the role of electrode capacitance on the initiation of pits for A516 carbon steel by electrochemical noise measurements. Corros Sci. 1999;41-7(7):1245–1256.
[62] Xia D, Song S, Wang J, et al. Determination of corrosion types from electrochemical noise by phase space reconstruction theory. Electrochem Commun. 2012;15(1):88–92.
[63] Cuevas-Arteaga C, Concha-Guzmán MO. Corrosion study of SS-316L exposed to LiBr–H_2O solution applying electrochemical techniques and weight loss method. Corrosion Engineering Science and Technology. 2009;44-1(1):57–68.
[64] Mansfeld F, Han LT, Lee CC, et al. Analysis of electrochemical impedance and noise data for polymer coated metals. Corros Sci. 1997;39-2(2):255–279.
[65] Mansfeld F, Sun A, Speckert E, et al., Electrochemical noise analysis (ENA) for active and passive systems, CORROSION/2000, (NACE-International), paper 418, pp. 418/1-418/11, (2000).
[66] Mansfeld F, Lee CC, Zhang G. Comparison of electrochemical impedance and noise data in the frequency domain. Electrochim Acta. 1998;43(3–4):435–438.
[67] ASTM Standard G102: practice for calculation of corrosion rates and related information from electrochemical measurements, 1994.

[68] Cuevas-Arteaga C. Corrosion Evaluation of AISI-309 Exposed to 50 mol% Na_2SO_4–50 mol% V_2O_5 at high temperature applying electrochemical techniques and the weight loss method. Int. Journal of Electrochemical Science. 2012;7:12283–12300.
[69] Cuevas-Arteaga C. Kinetics corrosion of SS-304 stainless steel exposed to lithium bromide aqueous solution at low temperatures. Rev. Mex. Ing. Quim.. 2006;5:27–45.
[70] Cuevas-Arteaga C, Porcayo-Calderón J. Electrochemical noise analysis in the frequency domain and determination of corrosion rates for SS-304 stainless steel Mater. Sci Eng A. 2006;435-436:439–446.
[71] Tiwari SN, Prakash S, Studies on the hot corrosion behaviour of some superalloys in Na_2SO_4-60% V_2O_5, Paper Presented at Symposium on Localized Corrosion and Environmental Cracking (SOLCEC), C-33, Kalpakkam, India, 1997.
[72] Raman RKS, Muddle BC. Role of high temperature corrosion in life assessment and microstructural degradation of Cr-Mo steel weldments. Int. J. Press. Vessel Piping. 2000;77: 117–123.
[73] Wilson R, Understanding and preventing fuel ash corrosion, CORROSION/76 (NACE International), Paper 12, pp. 12/1-12/23, (1976).
[74] Rapp RA. Chemistry and electrochemistry of hot corrosion of metals. Mat Sci Eng. 1987;87:319–327.
[75] Zhang YS, Rapp RA. Solubilities of CeO_2, HfO_2 and Y_2O_3 in fused Na_2SO_4-30 mol% NaVO3 and CeO_2 in pure Na_2SO_4 at 900 C. Corrosion. 1987;43(6):348–352.
[76] Wong-Moreno A, López-López D, Argote Mingram H, et al. Erosion, corrosion and deposits in gas turbines burning heavy, high sulphur fuel oil. Corrosion Rev. 1996;14-3(3–4):265–296.
[77] Du G, Li J, Wang WK, et al. Detection and characterization of stress-corrosion cracking on 304 stainless steel by electrochemical noise and acoustic emission techniques. Corros Sci. 2011;53-9(9):2918–2926.
[78] Pantony DA, Vasu KI. Studies in the corrosion of metals under melts - III. Kinetics of the corrosion of pure metals under molten vanadium pentoxide. Journal Inorganic Nuclear Chemistry. 1967;30(3):755–779.
[79] Pantony DA, Vasu KI. Studies in the corrosion of metals Under Melts - I. Theoretical survey of fireside corrosion of boilers and gas-turbines in the presence of vanadium pentoxide. Journal Inorganic Nuclear Chemistry. 1967;30(2):423–432.
[80] Opila EJ. High temperature materials corrosion challenges for energy conversion technologies. Electrochem Soc Int. 2013;22(4):69–73.
[81] Peters KR, Whittle DP, Stringer J. Oxidation and hot corrosion of nickel-based alloys containing molybdenum. Corros Sci. 1976;16(11):791–804.
[82] Fryburg GC, Kohl FJ, Stearns CA, et al. Chemical reactions involved in the initiation of hot corrosion of B-1900 and NASA-TRW VIA. J Electrochem Soc. 1982;129(3):571–585.
[83] Priyantha N, Jayaweera P, Sanjurjo A, et al. Corrosion-resistant metallic coatings for applications in highly aggressive environment. Surf Coat Technol. 2003;163/164:31–36.